Synergistic Toughening of Bioinspired Poly(vinyl alcohol)–Clay–Nanofibrillar Cellulose Artificial Nacre

Jianfeng Wang,[†] Qunfeng Cheng,[†,*] Ling Lin,[‡] and Lei Jiang[†]

[†]Key Laboratory of Bio-inspired Smart Interfacial Science and Technology of Ministry of Education, Beijing Key Laboratory of Bio-inspired Energy Materials and Devices, School of Chemistry and Environment, BeiHang University Beijing 100191, People's Republic of China and [‡]Engineering Research Center of Marine Biological Resource Comprehensive Utilization, SOA, The Third Institute of Oceanography of the State Oceanic Administration, Xiamen 361000, People's Republic of China

ABSTRACT Inspired by the layered aragonite platelet/nanofibrillar chitin/protein ternary structure and integration of extraordinary strength and toughness of natural nacre, artificial nacre based on clay platelet/nanofibrillar cellulose/poly(vinyl alcohol) is constructed through an evaporation-induced self-assembly technique. The synergistic toughening effect from clay platelets and nanofibrillar cellulose is successfully demonstrated. The artificial nacre achieves an excellent balance of strength and toughness and a fatigue-resistant property, superior to natural nacre and other conventional layered clay/polymer binary composites.

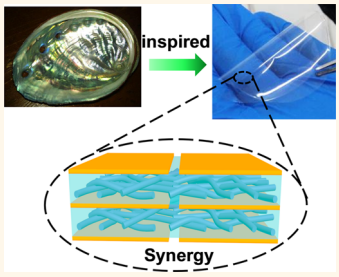

KEYWORDS: synergistic toughening · bioinspired · clay · artificial nacre · mechanical properties

Natural nacre has a nano/microscale hierarchical structure and precise inorganic–organic interface,[1–3] which enables it to achieve a unique combination of light weight, remarkable strength, and toughness.[4–7] From a mechanical point of view, nacre is often simplified as a binary composite, in which hard, two-dimensional (2D) aragonite platelets and soft biopolymer layers are alternately stacked into a brick-and-mortar structure.[8–10] Thus far, intense efforts have been devoted to mimicking the brick-and-mortar microstructure of nacre by assembling different types of 2D inorganic platelets and polymer matrices.[11–20] These bioinspired layered composites display impressive strength, which is commonly attributed to high filler content, compact layered structure, and a robust inorganic–organic interface.[21–27] In fact, more accurately, nacre should be regarded as a ternary composite, which consists of 2D aragonite platelets, one-dimensional (1D) nanofibrillar chitin, and protein.[28–30] The 2D aragonite platelets and 1D nanofibrillar chitin network layers are alternately stacked and held together by a soft protein adhesive.[31–33] Because the rigid nanofibrillar chitin is several nanometers in diameter, it has an enormous interface area. Thus, despite a relatively small amount of chitin compared to the thick aragonite platelets, the rigid nanofibrillar chitin plays an important role not only in the hierarchical control of the biomineralization process but in the mechanical support.[34,35] Obviously, the 2D and 1D building blocks act in a synergistic fashion for extraordinary strength and toughness balance through sliding of platelets and fiber, crack deflection, and crack bridging,[36,37] which supplies a novel inspiration for optimizing the mechanical properties of artificial nacre through the synergistic interaction of building blocks with different sizes and shapes.[38]

Herein, inspired by the layered aragonite platelet/nanofibrillar chitin/protein structure of nacre, artificial nacre based on montmorillonite platelet/nanofibrillar cellulose/poly(vinyl alcohol) (MMT/NFC/PVA) through an evaporation-induced assembly technique was constructed.[39,40] The synergistic toughening effect from MMT and NFC was successfully demonstrated in the artificial nacre, resulting in the integration of high strength and toughness. The artificial nacre achieves an excellent balance of strength and toughness and a fatigue-resistant property, superior to natural nacre and other

* Address correspondence to cheng@buaa.edu.cn.

Received for review December 16, 2013 and accepted February 8, 2014.

Published online February 08, 2014
10.1021/nn406428n

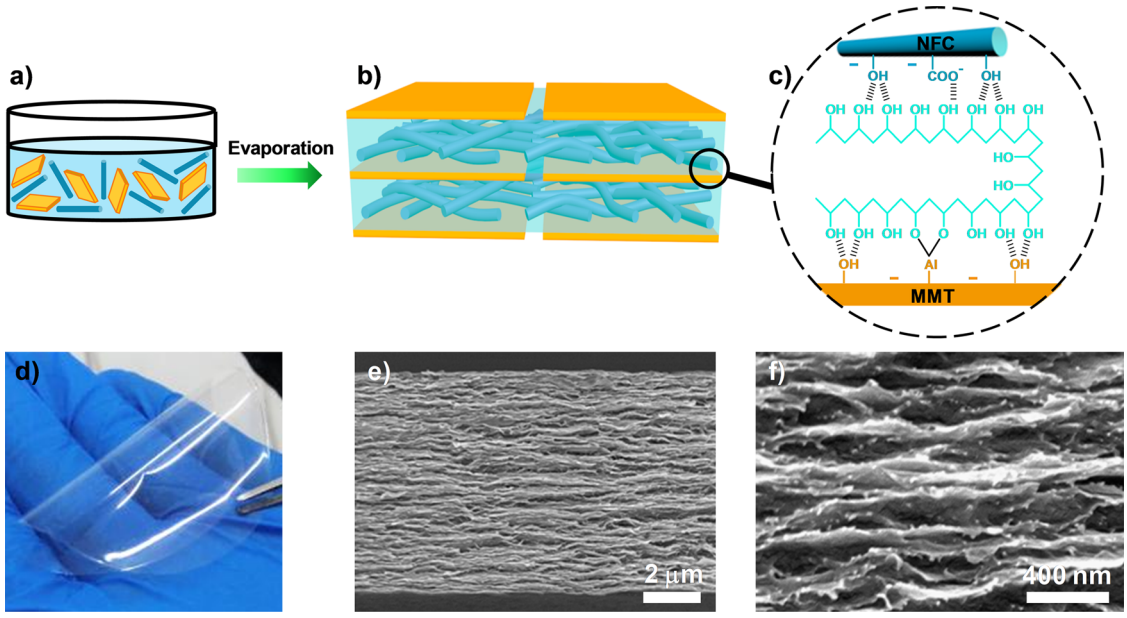

Scheme 1. (a) Fine aqueous dispersion of MMT platelets, NFC fibrils, and PVA, which were assembled into artificial nacre by evaporation. (b) Proposed structural model for the artificial nacre, in which MMT platelet and NFC fibril network layers are alternately stacked into a layered structure. (c) Anionic MMT platelets and anionic NFC fibrils are interconnected by PVA through hydrogen bonds and Al−O−C bonds. (d) Digital photo of artificial nacre, showing a high level of transparency. (e) Cross-section morphology of artificial nacre, showing a highly aligned layered arrangement. (f) Enlarged SEM image, showing homogeneous distribution of NFC fibrils (white dots).

conventional layered clay/polymer binary composites. The successful demonstration of synergistic toughening in our study supplies a novel way for designing and constructing high-performance bioinspired composites in the near future.

RESULTS AND DISCUSSION

NFC was prepared by 2,2,6,6-tetramethylpiperidine-1-oxyl (TEMPO)-mediated oxidation of microcrystalline cellulose.[41,42] The formed abundant sodium C6-carboxyl groups on the nanofibril surfaces greatly facilitated the separation of individual fibrils in water. The measured diameter of NFC fibrils is about 4.95 nm by atomic force microscopy (Supporting Information, Figure S1a). Nanoclay was substantially exfoliated by simple mechanical agitation in water, yielding individual MMT platelets with an average thickness of 1.28 nm (Supporting Information, Figure S1b).[40] Then, the PVA aqueous solution and the NFC suspension were added to the MMT suspension in turn and evaporated slowly (Scheme 1a). When the weight ratio of MMT to NFC is 1:2, a relatively good balance of strength and strain at break was achieved (Supporting Information, Figure S2). In addition, considering the density and statistical average thickness of exfoliated MMT and NFC, we controlled the mass ratio of MMT to NFC to be 1:2 and expected full NFC intercalation and separation of MMT platelets. According to our previous report,[40] we controlled the mass fraction of fillers (MMT and NFC) to be about 70 wt %, resulting in the perfect layered structure and high mechanical properties. The hybrid layered structure model of resultant artificial nacre is proposed as shown in Scheme 1b. The MMT platelets and NFC fibrils are adhered by PVA through strong hydrogen bonds and Al−O−C covalent bonds (Scheme 1c). The artificial nacre is highly transparent (Scheme 1d), and the transparency is about 90% at 600 nm (Supporting Information, Figure S3), which is comparable to the NFC/PVA hybrid film[43] and higher than other reported results,[44] due to complete exfoliation of clay.

A scanning electron microscopy (SEM) image shows the overall structure with a striking alignment of MMT platelets (Scheme 1e). NFC fibrils are distributed uniformly in the galleries of parallel MMT platelets (Scheme 1f). The intercalation of NFC fibrils into MMT galleries enlarges the interlayer distance between MMT, which is confirmed by X-ray diffraction (XRD) (Supporting Information, Figure S4). The interlayer distance of pure MMT film is about 1.26 nm (2θ = 7.1°). For the binary MMT/PVA composite, the interlayer distance of MMT platelets increases to about 3.4 nm (2θ = 2.6°). After incorporation of NFC fibrils, the reflection peak in the ternary MMT/NFC/PVA composite disappears in the range of 1.8° to 10°, indicating the successful insertion of NFC fibrils into MMT galleries. FTIR results indicate the connectivity between anionic NFC and anionic MMT by soft PVA through hydrogen bonds and Al−O−C covalent bonds (Supporting Information, Figure S5). In Figure S5a, the hydrogen bond peaks of MMT, NFC, and PVA are at 361, 3226, and 3333 cm^{-1}, respectively. For the MMT/NFC/PVA composite, the hydrogen bond peak shifts to 3336 cm^{-1}, which may be ascribed to the adsorption of PVA on the surface of MMT platelets and NFC

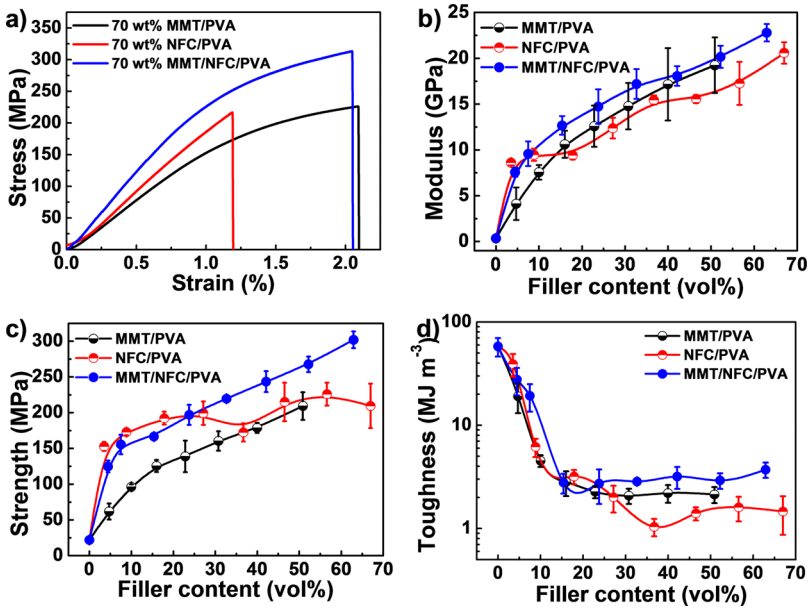

Figure 1. (a) Stress−strain curves of the artificial nacre and corresponding binary NFC/PVA and MMT/PVA composites containing 70 wt % fillers. (b−d) Tensile mechanical properties of MMT/NFC/PVA, NFC/PVA, and MMT/PVA composites with different amounts of fillers. The artificial nacre of the MMT/NFC/PVA shows excellent integration of strength and toughness, greater than the other binary composite of MMT/PVA and NFC/PVA, which is ascribed to the synegistic toughening effect from 2D MMT platelets and 1D NFC fibrils in the ternary artificial nacre.

fibrils. The new peak at 839 cm^{-1} of the MMT/NFC/PVA composite in Figure S5b indicates the formation of an Al−O−C bond between MMT and PVA.[21]

The above results confirm that our artificial nacre has a nacre-like structure, in which 2D MMT platelets and 1D NFC fibril network layers are stacked alternately and glued together effectively by PVA adhesive.

The tensile stress−strain curves of the nacre-inspired composite are shown in Figure 1a. The artificial nacre shows excellent integration of strength and toughness, greater than other binary composites. The tensile strength, Young's modulus, and toughness reach 302 ± 12 MPa, 22.8 ± 1.0 GPa, and 3.72 ± 0.63 MJ m^{-3}, respectively. Both the strength and toughness are 2 times higher than those of natural nacre (80−135 MPa and 1.8 MJ m^{-3}).[45] Similar to a previous report,[40] the binary MMT/PVA composite exhibits a layered structure (Supporting Information, Figure S6), and the NFC/PVA composite shows a random structure with uniform dispersion of NFC fibrils (Supporting Information, Figure S7). The corresponding tensile strength and toughness of MMT/PVA and NFC/PVA composites are 219 ± 19 MPa and 2.14 ± 0.30 MJ m^{-3} and 223 ± 31 MPa and 1.46 ± 0.59 MJ m^{-3}, respectively, which are lower than that of the artificial nacre. Obviously, the synergistic toughening from 2D MMT platelets and 1D NFC fibrils occurred in the ternary artificial nacre.

To understand the synergistic toughening mechanism, the mechanical properties of MMT/PVA, NFC/PVA, and MMT/NFC/PVA composites with different filler content (0−70 wt %) were measured, as shown in Figure 1b−d. The volume fraction of fillers is calculated by using the weight fraction and density of MMT (2.86 g cm^{-3}), NFC (1.46 g cm^{-3}), and PVA (1.27 g cm^{-3}), respectively. The strength changes in the range of high filler content show distinct trends from the modulus (Figure 1b). The strength of NFC/PVA composites seems to be saturated, while that of MMT/PVA composites is enhanced gradually, due to the ordered layered structure (Figure 1c).[40] For MMT/NFC/PVA composites, both high reinforcement efficiency and the ability to incorporate high filler content are achieved. These indicate that the layered structure with alternate stacking of 2D MMT platelet and 1D NFC fibril network layers contributes to the synergistic strength of artificial nacre.

The other contribution to the synergistic strength of artificial nacre is the interconnectivity between MMT and NFC through PVA. If PVA adhesive is absent, the MMT platelets tend to aggregate (Supporting Information, Figure S8).[44,46] The interaction between anionic MMT and anionic NFC is relatively weak (Supporting Information, Figure S5). In addition, both MMT and NFC are quite rigid. Direct stress transfer between two rigid components is often deficient, as indicated by multiple recent studies.[47−49] As a result, the MMT/NFC composite without PVA exhibits relatively weak mechanical properties with a Young's modulus of 19.6 ± 1.0 GPa and a tensile strength of 223 ± 28 MPa (Supporting Information, Figure S9). The contrast comparsion clearly shows the importance of PVA adhesion between MMT and NFC in the artificial nacre.

For platelet-shaped reinforcements, toughness can be greatly improved by platelet-induced crack deflection, which leads to tortuous fracture path.[50] This is recognized as the most prominent toughening mechanism in nacre.[51] Compared with 1D fibers, 2D platelets are

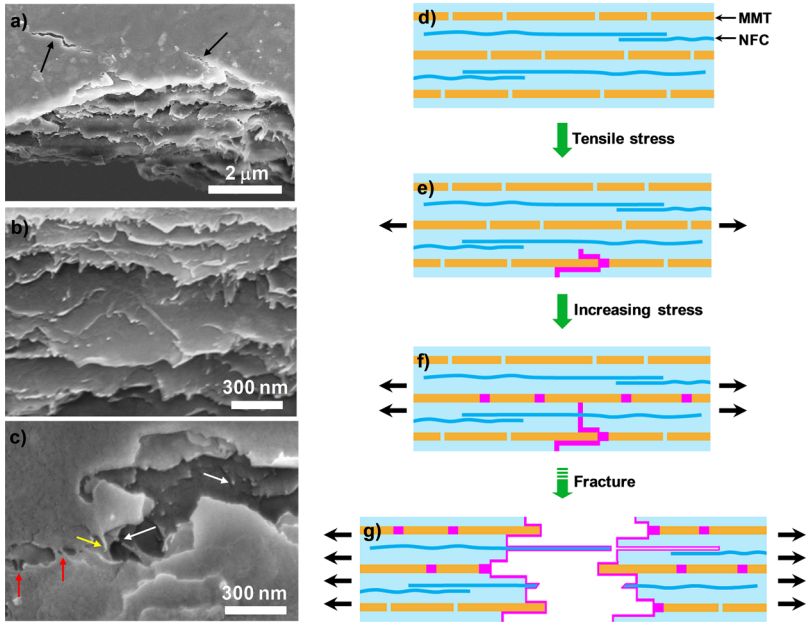

Figure 2. (a–c) Fracture morphology of the artificial nacre. (a) Microcrack divergence, (b) MMT platelet pull-out on fracture surface, and (c) crack bridging, fibril pull-out, and fracture at the tip of a microcrack. (d–g) Proposed synergistic mechanism of 2D MMT platelets and 1D NFC fibrils. (d) Simplified structural schematics, showing the alternate arrangement of NFC fibril layers and MMT platelets. (e) Under tensile stress, the MMT platelet starts to slide and deflect crack. (f) NFC fibril bridges the crack and offers resistance to MMT sliding, which activates potential sliding sites of multiple MMT platelets in the next layer. (g) The composite finally fails under MMT pull-out and NFC pull-out/fracture mode.

more effective for crack deflection, which was demonstrated theoretically and experimentally.[52] In this study, the MMT/PVA composites are indeed tougher than the NFC/PVA composites at high filler content (Figure 1d). Interestingly, the fracture energies of ternary MMT/NFC/PVA composites are larger than those of corresponding binary composites. To explore the mechanism of the toughness, fracture morphology of the artificial nacre is carefully examined, as shown in Figure 2a–c. The MMT platelets are pulled out and the NFC fibrils fracture in the process of tensile testing (Figure 2b). Some divergent microcracks emerge on the surface of the MMT/NFC/PVA composite (Figure 2a). At the tip of microcracks, crack bridging, fibril pull-out, and fracture are observed (Figure 2c). The feature of the fracture surface indicates that MMT platelet sliding happens not only on the fracture surface but also in the interior of the MMT/NFC/PVA composite, which may be responsible for the improved fracture energy of the MMT/NFC/PVA composite.

In terms of the fracture morphology of the artificial nacre, a crack extension model is proposed to illustrate the synergistic toughening of 2D MMT platelets and 1D NFC fibrils, as shown in Figure 2d–g. First, a deflected crack induced by an MMT platelet encounters an NFC fibril (Figure 2e). Then, the NFC fibril bridges the crack. The bridging NFC fibril can generate obvious resistance to the sliding of adjacent MMT platelets (strain hardening). The enhanced stress is transferred to next layer of MMT platelets and activates the potential sliding of adjacent multiple MMT platelets (Figure 2f). With crack extension, such crack deflection, bridging, and activation of multiple potential sliding sites are accumulative in a step fashion until the material fractures. This deformation process is also reflected by the strain hardening in the nonlinear stress–strain curve (Figure 1a) and is akin to the deformation of hydrated nacre.[2,53] Finally, the material fails under platelet pull-out and fibril pull-out/fracture mode (Figure 2g). In this way, energy dissipation through cooperative sliding of MMT and NFC pervades through a relatively large volume, rather than only at the fracture surface, leading to the synergistic toughness. At the same time, the fibril pull-out/fracture mode also helps to improve the strength of artificial nacre.

A comparison of mechanical performance of our artificial nacre with those of natural nacre and reported layered clay/polymer composites with high filler content is shown in Figure 3. The detailed data are listed in Table S1. Obviously, the artificial nacre exhibits a better balance of strength and toughness. The strength is 1.2–6.2 times higher than those of layered binary clay/polymer composites without cross-linking (red triangles).[13,22,23,46,54–57] The toughness is 2.2–7 times higher than those of layered binary clay/polymer composites with covalent or ionic cross-linking (blue triangles).[21–23,57,58] The integrated mechanical properties are far superior to natural nacre (black square)[45] and ternary MMT/NFC/chitosan composite (green circle).[59] The synergy between 2D MMT platelets and 1D NFC fibrils is mostly responsible for improving the strength and toughness simultaneously. Differently, covalent or ionic cross-linking is prone to improve

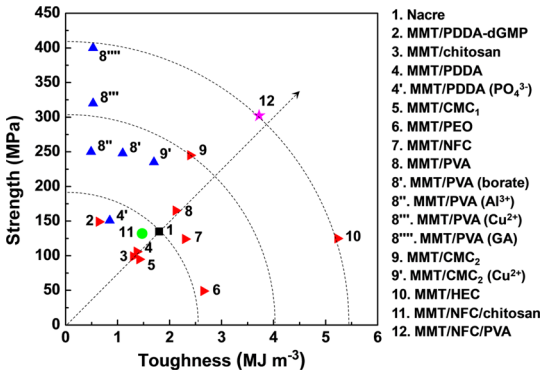

Figure 3. Comparison of mechanical properties of our artificial nacre of an MMT/NFC/PVA composite with natural nacre and the reported layered clay/polymer composites. The dashed borders separate regions with improving integrated properties. The arrow connecting the origin of the coordinate and the point of nacre shows the overall desired direction for properties of bioinspired nanocomposites. (Nomenclature: Filler/matrix (cross-linker). Abbreviations: PDDA, poly(diallyldimethyl-ammonium chloride); dGMP, 2′-deoxyguanosine 5′-monophosphates; CMC, sodium carboxymethyl cellulose; PEO, polyethylene oxide; GA, glutaraldehyde; HEC, hydroxyethylcellulose.)

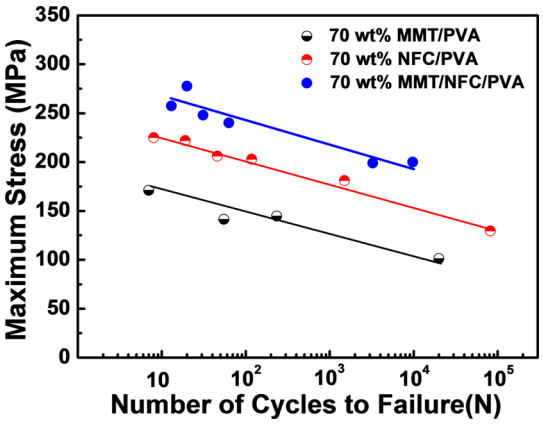

Figure 4. Maximum stress (*S*) *vs* number of cycles to failure (*N*) in pure tension mode (*i.e.*, no compressive stress) for the artificial nacre and corresponding binary NFC/PVA and MMT/PVA composites.

strength at the expense of toughness due to increased restriction of mutual movement of clay platelets in deformation. For example, although the MMT/PVA composite treated with glutaraldehyde shows a very high strength of 400 MPa, the toughness is reduced to only 0.53 MJ m^{-3}.[21] On the contrary, choosing ductile polymer and designing its soft interfacial interaction with clay platelets tend to increase the strain at break and thus toughness, but compromise strength, due to facilitation of mutual sliding of clay platelets and concomitant plastic deformation of the polymer. For example, an MMT/hydroxyethylcellulose composite with 60 wt % clay has a remarkable strain at break of 6.8% and toughness of about 5.23 MJ m^{-3}, while the strength is as low as 125 MPa.[56]

The artificial nacre and corresponding binary composites were also fatigue tested in tension mode. The frequency of the cyclic loading tests was 0.5 Hz, and the stress ratio (*R*: minimum to maximumu applied stress) was 0.1.[60] The maximum tensile stress (*S*) *vs* the number of cycles to failure (*N*) was ploted as *S*−*N* curves, shown in Figure 4. The fatigue results indicate that the artificial nacre has much better fatigue-resistance than the corresponding MMT/PVA and NFC/PVA binary composites. At same stress level, the fatigue life of artificial nacre is 2 and 4 orders of magnitude higher than the NFC/PVA and MMT/PVA composites, respectively, further verifying the synergistic toughening effect from clay platelets and nanofibrillar cellulose. As previously reported,[52,60,61] 2D nanoplatelets suppress crack propagation by crack deflection and thus increase fracture surface area during crack growth, and 1D nanofibrils suppress crack propagation by crack bridging and subsequent pull-out of nanofibrils.[62−64] In the artificial nacre of the MMT/NFC/PVA composite, the two crack suppression mechanisms synergistically act, which increases energy dissipation and thus prolongs fatigue life.

CONCLUSION

In conclusion, inspired by the ternary structure of nacre with layered aragonite platelet/nanofibrillar chitin/protein, we successfully constructed high-performance artificial nacre. The synergistic toughening effect from clay platelets and nanofibrillar cellulose was successfully demonstrated. The artificial nacre achieves high fatigue life and excellent balance of strength and toughness, superior to natural nacre and other conventional layered clay/polymer binary composites. On the other hand, the ordered nanostructure of the artificial nacre enables it to achieve extraordinary optical transparency. These findings provide a new concept for design and constructing of high-performance composites based on nanoclay for applications, such as flexible electronics, precision optical devices, and food packaging. Looking out to the future, the present bioinspired synergistic concept of 2D platelet and 1D nanofiber can be applied to other strong 2D and 1D building blocks, such as graphene, alumina platelets, carbon nanotubes, and Kevlar nanofiber. We believe that the ternary nacre-like structure consisting of 2D platelets and 1D nanofibers will promote bioinspired composites toward integration of high strength, toughness, and fatigue life.

METHODS

Raw Materials. PVA (M_w = 146 000−186 000), cellulose powder (microcrystalline), sodium bromide, sodium hypochlorite solution (available chlorine 10−15%), and TEMPO (98%) were purchased from Sigma-Aldrich. Na^+-type MMT was supplied by Zhejiang Fenghong Clay Co. Ltd. TEMPO-oxidized NFC was prepared using a TEMPO/NaBr/NaClO system[41] in water at pH 10 and room temperature under the conditions reported in the

literature.[42] The obtained transparent NFC aqueous solution was weighed, dried, and reweighed to determine NFC mass concentration. MMT was exfoliated in water by mechanically stirring according to the literature.[40] The concentrations of the transparent NFC and MMT suspensions were adjusted to 0.27 wt %. The MMT platelets have an average lateral size of 119 nm and an average thickness of 1.28 nm. The length and average diameter of the NFC fibrils are measured to be 300−800 and 4.95 nm, respectively.

Preparation of MMT/NFC/PVA Composites. A desired amount of PVA solution (0.5 wt %) was gradually added to a stirred MMT dispersion. After slowly stirring for 3 h, a desired amount of NFC suspension was added and continually stirred for 3 h. Finally, the homogeneous mixture was poured into a culture dish and kept at room temperature for film formation until its weight equilibrated. This film was peeled off from the bottom of the dish. A series of MMT/NFC/PVA films with different filler weight fraction were prepared by varying the weight of PVA, MMT, and NFC dispersions. In all films, the mass ratio of MMT to NFC was constantly controlled to be 1:2. MMT/PVA and NFC/PVA films with different filler weight fraction were also prepared by the same evaporation process.

Characterization. The tensile mechanical properties were evaluated using a Shimadzule AGS-X Tester at a load speed of 0.5 mm min^{-1} with a gauge length of 10 mm. All of the samples were cut into strips with the width of 3 mm and length of 30 mm. The SEM images were obtained by a JEOL JSM-7500. XRD experiments were carried out with a Panalytical Empyrean instrument using Cu Kα radiation. Atomic force microscope images were acquired by the Veeco Multimode VIII. Light transmittance spectroscopy of the film was measured using a Hitachi U-4100 UV−vis spectrophotometer. FTIR spectra were collected by a Bruker Tensor-27 utilizing the attenuated total internal reflectance accessory. The tensile fatigue tests were performed at a frequency of 0.5 Hz using the Instron ElectroPuls E1000 test facility. The ratio of the minimum applied stress to maximum stress ratio was set at 0.1.

Conflict of Interest: The authors declare no competing financial interest.

Acknowledgment. This work was supported by the National Research Fund for Fundamental Key Projects (2010CB934700), the National Natural Science Foundation of China (21273017, 51103004), Program for New Century Excellent Talents in University (NCET-12-0034), Beijing Nova Program (Z121103002512020), Beijing Science and Technology Program (Z121100001312004), the Key Research Program of the Chinese Academy of Sciences (KJZD-EW-M01), Opening Project of the Beijing National Laboratory for Molecular Sciences (BNLMS) and the 111 Project (No. B14009). The authors thank Dr. Yuanyuan Shang from Peking University for her kind assistance in fatigue testing.

Supporting Information Available: AFM images, light transmittance spectroscopy, XRD curves, FTIR spectra, SEM images, stress−strain curves, and table for comparison of mechanical properties. This material is available free of charge *via* the Internet at http://pubs.acs.org.

REFERENCES AND NOTES

1. Yao, H.-B.; Fang, H.-Y.; Wang, X.-H.; Yu, S.-H. Hierarchical Assembly of Micro-/nano-Building Blocks: Bio-inspired Rigid Structural Functional Materials. *Chem. Soc. Rev.* **2011**, *40*, 3764–3785.
2. Wang, J.; Cheng, Q.; Tang, Z. Layered Nanocomposites Inspired by the Structure and Mechanical Properties of Nacre. *Chem. Soc. Rev.* **2012**, *41*, 1111–1129.
3. Espinosa, H. D.; Rim, J. E.; Barthelat, F.; Buehler, M. J. Merger of Structure and Material in Nacre and Bone-Perspectives on *de Novo* Biomimetic Materials. *Prog. Mater. Sci.* **2009**, *54*, 1059–1100.
4. Huang, Z.; Li, H.; Pan, Z.; Wei, Q.; Chao, Y. J.; Li, X. Uncovering High-Strain Rate Protection Mechanism in Nacre. *Sci. Rep.* **2011**, *1*, 148.
5. Huang, Z. W.; Li, X. D. Order-Disorder Transition of Aragonite Nanoparticles in Nacre. *Phys. Rev. Lett.* **2012**, *109*, 025501.
6. Li, X. D.; Huang, Z. W. Unveiling the Formation Mechanism of Pseudo-Single-Crystal Aragonite Platelets in Nacre. *Phys. Rev. Lett.* **2009**, *102*, 075502.
7. Li, X.; Xu, Z.-H.; Wang, R. *In Situ* Observation of Nanograin Rotation and Deformation in Nacre. *Nano Lett.* **2006**, *6*, 2301–2304.
8. Jackson, A. P.; Vincent, J. F. V.; Turner, R. M. The Mechanical Design of Nacre. *Proc. R. Soc. London B* **1988**, *234*, 415–440.
9. Gao, H.; Ji, B.; Jäger, I. L.; Arzt, E.; Fratzl, P. Materials Become Insensitive to Flaws at Nanoscale: Lessons from Nature. *Proc. Natl. Acad. Sci. U.S.A.* **2003**, *100*, 5597–5600.
10. Mayer, G. Rigid Biological Systems as Models for Synthetic Composites. *Science* **2005**, *310*, 1144–1147.
11. Tang, Z.; Kotov, N. A.; Magonov, S.; Ozturk, B. Nanostructured Artificial Nacre. *Nat. Mater.* **2003**, *2*, 413–418.
12. Bonderer, L. J.; Studart, A. R.; Gauckler, L. J. Bioinspired Design and Assembly of Platelet Reinforced Polymer Films. *Science* **2008**, *319*, 1069–1073.
13. Yao, H.-B.; Tan, Z.-H.; Fang, H.-Y.; Yu, S.-H. Artificial Nacre-like Bionanocomposite Films from the Self-Assembly of Chitosan−Montmorillonite Hybrid Building Blocks. *Angew. Chem., Int. Ed.* **2010**, *49*, 10127–10131.
14. Yao, H.-B.; Fang, H.-Y.; Tan, Z.-H.; Wu, L.-H.; Yu, S.-H. Biologically Inspired, Strong, Transparent, and Functional Layered Organic−Inorganic Hybrid Films. *Angew. Chem., Int. Ed.* **2010**, *49*, 2140–2145.
15. Wang, J.; Lin, L.; Cheng, Q.; Jiang, L. A Strong Bio-Inspired Layered PNIPAM−Clay Nanocomposite Hydrogel. *Angew. Chem., Int. Ed.* **2012**, *51*, 4676–4680.
16. Cheng, Q.; Wu, M.; Li, M.; Jiang, L.; Tang, Z. Ultratough Artificial Nacre Based on Conjugated Cross-linked Graphene Oxide. *Angew. Chem., Int. Ed.* **2013**, *52*, 3750–3755.
17. Kochumalayil, J. J.; Bergenstråhle-Wohlert, M.; Utsel, S.; Wågberg, L.; Zhou, Q.; Berglund, L. A. Bioinspired and Highly Oriented Clay Nanocomposites with a Xyloglucan Biopolymer Matrix: Extending the Range of Mechanical and Barrier Properties. *Biomacromolecules* **2012**, *14*, 84–91.
18. Podsiadlo, P.; Liu, Z.; Paterson, D.; Messersmith, P. B.; Kotov, N. A. Fusion of Seashell Nacre and Marine Bioadhesive Analogs: High-Strength Nanocomposite by Layer-by-Layer Assembly of Clay and L-3,4-Dihydroxyphenylalanine Polymer. *Adv. Mater.* **2007**, *19*, 949–955.
19. Hu, X.; Xu, Z.; Gao, C. Multifunctional, Supramolecular, Continuous Artificial Nacre Fibres. *Sci. Rep.* **2012**, *2*, 767.
20. Erb, R. M.; Libanori, R.; Rothfuchs, N.; Studart, A. R. Composites Reinforced in Three Dimensions by Using Low Magnetic Fields. *Science* **2012**, *335*, 199–204.
21. Podsiadlo, P.; Kaushik, A. K.; Arruda, E. M.; Waas, A. M.; Shim, B. S.; Xu, J.; Nandivada, H.; Pumplin, B. G.; Lahann, J.; Ramamoorthy, A.; *et al.* Ultrastrong and Stiff Layered Polymer Nanocomposites. *Science* **2007**, *318*, 80–83.
22. Walther, A.; Bjurhager, I.; Malho, J.-M.; Pere, J.; Ruokolainen, J.; Berglund, L. A.; Ikkala, O. Large-Area, Lightweight and Thick Biomimetic Composites with Superior Material Properties *via* Fast, Economic, and Green Pathways. *Nano Lett.* **2010**, *10*, 2742–2748.
23. Walther, A.; Bjurhager, I.; Malho, J.-M.; Ruokolainen, J.; Berglund, L.; Ikkala, O. Supramolecular Control of Stiffness and Strength in Lightweight High-Performance Nacre-Mimetic Paper with Fire-Shielding Properties. *Angew. Chem., Int. Ed.* **2010**, *49*, 6448–6453.
24. Li, Y.-Q.; Yu, T.; Yang, T.-Y.; Zheng, L.-X.; Liao, K. Bio-Inspired Nacre-like Composite Films Based on Graphene with Superior Mechanical, Electrical, and Biocompatible Properties. *Adv. Mater.* **2012**, *24*, 3426–3431.
25. Huang, L.; Li, C.; Yuan, W.; Shi, G. Strong Composite Films with Layered Structures Prepared by Casting Silk Fibroin-Graphene Oxide Hydrogels. *Nanoscale* **2013**, *5*, 3780–3786.
26. Hu, X.; Xu, Z.; Liu, Z.; Gao, C. Liquid Crystal Self-templating Approach to Ultrastrong and Tough Biomimic Composites. *Sci. Rep.* **2013**, *3*, 2374.
27. Zhao, X.; Xu, Z.; Zheng, B.; Gao, C. Macroscopic Assembled, Ultrastrong and H_2SO_4-Resistant Fibres of Polymer-Grafted Graphene Oxide. *Sci. Rep.* **2013**, *3*, 3164.

28. Weiner, S.; Traub, W.; Parker, S. B. Macromolecules in Mollusc Shells and Their Functions in Biomineralization [and Discussion]. *Philos. Trans. R. Soc., B* **1984**, *304*, 425–434.
29. Levi-Kalisman, Y.; Falini, G.; Addadi, L.; Weiner, S. Structure of the Nacreous Organic Matrix of a Bivalve Mollusk Shell Examined in the Hydrated State Using Cryo-TEM. *J. Struct. Biol.* **2001**, *135*, 8–17.
30. Nudelman, F.; Chen, H. H.; Goldberg, H. A.; Weiner, S.; Addadi, L. Spiers Memorial Lecture Lessons from Biomineralization: Comparing the Growth Strategies of Mollusc Shell Prismatic and Nacreous Layers in Atrina Rigida. *Faraday Discuss.* **2007**, *136*, 9–25.
31. Furuhashi, T.; Schwarzinger, C.; Miksik, I.; Smrz, M.; Beran, A. Molluscan Shell Evolution with Review of Shell Calcification Hypothesis. *Comp. Biochem. Phys. B* **2009**, *154*, 351–371.
32. Suzuki, M.; Saruwatari, K.; Kogure, T.; Yamamoto, Y.; Nishimura, T.; Kato, T.; Nagasawa, H. An Acidic Matrix Protein, Pif, Is a Key Macromolecule for Nacre Formation. *Science* **2009**, *325*, 1388–1390.
33. Laaksonen, P.; Walther, A.; Malho, J.-M.; Kainlauri, M.; Ikkala, O.; Linder, M. B. Genetic Engineering of Biomimetic Nanocomposites: Diblock Proteins, Graphene, and Nanofibrillated Cellulose. *Angew. Chem., Int. Ed.* **2011**, *50*, 8688–8691.
34. Meyers, M. A.; Chen, P.-Y.; Lin, A. Y.-M.; Seki, Y. Biological Materials: Structure and Mechanical Properties. *Prog. Mater. Sci.* **2008**, *53*, 1–206.
35. Chen, P. Y.; McKittrick, J.; Meyers, M. A. Biological Materials: Functional Adaptations and Bioinspired Designs. *Prog. Mater. Sci.* **2012**, *57*, 1492–1704.
36. Ritchie, R. O. The Conflicts between Strength and Toughness. *Nat. Mater.* **2011**, *10*, 817–822.
37. Launey, M. E.; Ritchie, R. O. On the Fracture Toughness of Advanced Materials. *Adv. Mater.* **2009**, *21*, 2103–2110.
38. Lu, H.; Chen, Z.; Ma, C. Bioinspired Approaches for Optimizing the Strength and Toughness of Graphene-Based Polymer Nanocomposites. *J. Mater. Chem.* **2012**, *22*, 16182–16190.
39. Das, P.; Schipmann, S.; Malho, J.-M.; Zhu, B.; Klemradt, U.; Walther, A. Facile Access to Large-Scale, Self-Assembled, Nacre-Inspired, High-Performance Materials with Tunable Nanoscale Periodicities. *ACS Appl. Mater. Interfaces* **2013**, *5*, 3738–3747.
40. Wang, J.; Cheng, Q.; Lin, L.; Chen, L.; Jiang, L. Understanding the Relationship of Performance with Nanofiller Content in the Biomimetic Layered Nanocomposites. *Nanoscale* **2013**, *5*, 6356–6362.
41. Saito, T.; Nishiyama, Y.; Putaux, J.-L.; Vignon, M.; Isogai, A. Homogeneous Suspensions of Individualized Microfibrils from TEMPO-Catalyzed Oxidation of Native Cellulose. *Biomacromolecules* **2006**, *7*, 1687–1691.
42. Okita, Y.; Saito, T.; Isogai, A. Entire Surface Oxidation of Various Cellulose Microfibrils by TEMPO-Mediated Oxidation. *Biomacromolecules* **2010**, *11*, 1696–1700.
43. Yano, H.; Sugiyama, J.; Nakagaito, A. N.; Nogi, M.; Matsuura, T.; Hikita, M.; Handa, K. Optically Transparent Composites Reinforced with Networks of Bacterial Nanofibers. *Adv. Mater.* **2005**, *17*, 153–155.
44. Wu, C.-N.; Saito, T.; Fujisawa, S.; Fukuzumi, H.; Isogai, A. Ultrastrong and High Gas-Barrier Nanocellulose/Clay-Layered Composites. *Biomacromolecules* **2012**, *13*, 1927–1932.
45. Wang, R. Z.; Suo, Z.; Evans, A. G.; Yao, N.; Aksay, I. A. Deformation Mechanisms in Nacre. *J. Mater. Res.* **2001**, *16*, 2485–2493.
46. Liu, A.; Walther, A.; Ikkala, O.; Belova, L.; Berglund, L. A. Clay Nanopaper with Tough Cellulose Nanofiber Matrix for Fire Retardancy and Gas Barrier Functions. *Biomacromolecules* **2011**, *12*, 633–641.
47. Podsiadlo, P.; Tang, Z.; Shim, B. S.; Kotov, N. A. Counterintuitive Effect of Molecular Strength and Role of Molecular Rigidity on Mechanical Properties of Layer-by-Layer Assembled Nanocomposites. *Nano Lett.* **2007**, *7*, 1224–1231.
48. Chen, P.; Yun, Y. S.; Bak, H.; Cho, S. Y.; Jin, H.-J. Multiwalled Carbon Nanotubes-Embedded Electrospun Bacterial Cellulose Nanofibers. *Mol. Cryst. Liq. Cryst.* **2010**, *519*, 169–178.
49. Lu, P.; Hsieh, Y.-L. Multiwalled Carbon Nanotube (MWCNT) Reinforced Cellulose Fibers by Electrospinning. *ACS Appl. Mater. Interfaces* **2010**, *2*, 2413–2420.
50. Faber, K. T.; Evans, A. G. Crack Deflection Processes. 1. Theory. *Acta Metall.* **1983**, *31*, 565–576.
51. Wang, R. Z.; Wen, H. B.; Cui, F. Z.; Zhang, H. B.; Li, H. D. Observations of Damage Morphologies in Nacre during Deformation and Fracture. *J. Mater. Sci.* **1995**, *30*, 2299–2304.
52. Rafiee, M. A.; Rafiee, J.; Srivastava, I.; Wang, Z.; Song, H.; Yu, Z.-Z.; Koratkar, N. Fracture and Fatigue in Graphene Nanocomposites. *Small* **2009**, *6*, 179–183.
53. Barthelat, F.; Tang, H.; Zavattieri, P. D.; Li, C. M.; Espinosa, H. D. On the Mechanics of Mother-of-Pearl: A Key Feature in the Material Hierarchical Structure. *J. Mech. Phys. Solids* **2007**, *55*, 306–337.
54. Martikainen, L.; Walther, A.; Seitsonen, J.; Berglund, L. A.; Ikkala, O. Deoxyguanosine Phosphate Mediated Sacrificial Bonds Promote Synergistic Mechanical Properties in Nacre-Mimetic Nanocomposites. *Biomacromolecules* **2013**, *14*, 2531–2535.
55. Liu, A.; Berglund, L. A. Fire-Retardant and Ductile Clay Nanopaper Biocomposites Based on Montmorrilonite in Matrix of Cellulose Nanofibers and Carboxymethyl Cellulose. *Eur. Polym. J.* **2013**, *49*, 940–949.
56. Sehaqui, H.; Kochumalayil, J.; Liu, A.; Zimmermann, T.; Berglund, L. A. Multifunctional Nanoclay Hybrids of High Toughness, Thermal, and Barrier Performances. *ACS Appl. Mater. Interfaces* **2013**, *5*, 7613–7620.
57. Das, P.; Walther, A. Ionic Supramolecular Bonds Preserve Mechanical Properties and Enable Synergetic Performance at High Humidity in Water-Borne, Self-Assembled Nacremimetics. *Nanoscale* **2013**, *5*, 9348–9356.
58. Podsiadlo, P.; Kaushik, A. K.; Shim, B. S.; Agarwal, A.; Tang, Z.; Waas, A. M.; Arruda, E. M.; Kotov, N. A. Can Nature's Design Be Improved Upon? High Strength, Transparent Nacre-Like Nanocomposites with Double Network of Sacrificial Cross Links. *J. Phys. Chem. B* **2008**, *112*, 14359–14363.
59. Liu, A.; Berglund, L. A. Clay Nanopaper Composites of Nacre-like Structure Based on Montmorrilonite and Cellulose Nanofibers—Improvements Due to Chitosan Addition. *Carbohydr. Polym.* **2012**, *87*, 53–60.
60. Yavari, F.; Rafiee, M. A.; Rafiee, J.; Yu, Z. Z.; Koratkar, N. Dramatic Increase in Fatigue Life in Hierarchical Graphene Composites. *ACS Appl. Mater. Interfaces* **2010**, *2*, 2738–2743.
61. Rafiee, M. A.; Rafiee, J.; Wang, Z.; Song, H.; Yu, Z. Z.; Koratkar, N. Enhanced Mechanical Properties of Nanocomposites at Low Graphene Content. *ACS Nano* **2009**, *3*, 3884–3890.
62. Zhang, W.; Picu, R. C.; Koratkar, N. Suppression of Fatigue Crack Growth in Carbon Nanotube Composites. *Appl. Phys. Lett.* **2007**, *91*, 193109.
63. Zhang, W.; Picu, R. C.; Koratkar, N. The Effect of Carbon Nanotube Dimensions and Dispersion on the Fatigue Behavior of Epoxy Nanocomposites. *Nanotechnology* **2008**, *19*, 285709.
64. Zhang, W.; Srivastava, I.; Zhu, Y. F.; Picu, C. R.; Koratkar, N. A. Heterogeneity in Epoxy Nanocomposites Initiates Crazing: Significant Improvements in Fatigue Resistance and Toughening. *Small* **2009**, *5*, 1403–1407.